Clays and Clay Minerals, Vol. 65, No. 3, 206–219, 2017.

SOLID-STATE ^{1}H AND ^{27}Al NMR STUDIES OF DMSO-KAOLINITE INTERCALATES

JONATHAN FAFARD, VICTOR TERSKIKH, AND CHRISTIAN DETELLIER*

Center for Catalysis Research and Innovation and Department of Chemistry and Biomolecular Sciences, University of Ottawa, Ottawa, Ontario K1N 6N5, Canada

Abstract—Nuclear magnetic resonance (NMR) provides a powerful tool to describe local nuclear environments. In this work, unique structural information on kaolinite and on kaolinite dimethylsulfoxide (DMSO) intercalate were provided by solid-state ^{1}H and ^{27}Al magic-angle spinning (MAS) NMR. The interlayer chemistry of kaolinite (K) was examined by intercalating a select group of highly polar organic molecules or salts into kaolinite as a first step. Once the interlayer space is expanded, the intercalated compounds can be replaced in a second step. Intercalating DMSO into kaolinite to form the DMSO-K intercalate is, thus, a particularly useful first step toward the intercalation of a large variety of molecules, including polymers and ionic liquids. Well developed characterization methods are essential to define the structural modifications of kaolinite, and MAS NMR is a useful complement to other techniques. The use of ^{1}H and ^{27}Al MAS NMR for this purpose has been relatively rare. ^{1}H NMR, nevertheless, can give unique information about kaolinite hydroxyls. Because quadrupolar interactions are sensitive to the local octahedral Al(III) geometry, solid-state ^{27}Al NMR can follow subtle structural modifications in the octahedral sheet. In the present work, the ^{1}H MAS NMR chemical shifts of KGa-1b were unambiguously attributed to the internal surface hydroxyls at 2.7 ppm and to the internal hydroxyls at 1.7 ppm. The ^{1}H MAS NMR chemical shifts of the two methyl groups in DMSO-K are not equivalent and can be attributed to the 2.9 and 4.2 ppm peaks. The ^{27}Al MAS NMR spectra of KGa-1b obtained under different magnetic fields revealed that most of the quadrupolar effects were highly reduced at 21.1 T, whereas the spectra at lower field, 4.7 T, were dominated by quadrupolar effects. The two octahedral Al(III) sites are not equivalent and can be distinguished in the low-field spectral simulation. Increased quadrupolar constants were observed and showed the major perturbations of the local Al symmetry that resulted from DMSO intercalation. Both the ^{1}H and ^{27}Al MAS NMR studies at different magnetic fields afforded important information about the local environments of the kaolinite hydroxyl groups and structural Al(III).

Key Words—^{27}Al MAS NMR, Deconvolution, DMSO, ^{1}H MAS, Intercalation, Kaolinite, Quadrupolar Interactions, Solid-State NMR

INTRODUCTION

Clay minerals are known for many unique chemical and physical properties that make them attractive starting materials for a vast variety of applications (Johnston, 2010; Bergaya and Lagaly, 2013). Kaolinite is very abundant in nature and large quantities are used in classical applications (*e.g.* paper coating, paint, ceramics, etc.) (Murray and Keller, 1993; Murray, 2007). Kaolinite plays a prominent role in human activities (Schroeder and Erickson, 2014). Hence, it is important to understand the kaolinite structural modifications and surface functionalization used to control a vast spectrum of applications and processes, such as catalysis and organic reactivity (Laszlo, 1986; Mccabe and Adams, 2013, Ngnie *et al*., 2016), clay-polymer nanocomposites (Letaief and Detellier, 2009; Galimberti *et al*., 2013), bitumen extraction from oil sands (Detellier *et al*., 2015; Lin *et al*., 2016), soil permeability and soil transport processes (Yong and Mourato, 1990), or the abiotic origin of life (Brack, 2013). In that context, well developed characterization methods are needed to precisely monitor kaolinite structural modifications that are related to intercalation. Kaolinite has potential uses in more specialized and advanced application niches if the interlayer chemistry that results from grafting or intercalating organic moieties can be better understood, mastered, and developed (Dedzo and Detellier, 2016). The kaolinite structure is one of the kaolin sub-group polytypes and is made of dioctahedral 1:1 layers with the $Al_2Si_2O_5(OH)_4$ general composition (Brigatti *et al*., 2013). The crystallographic structure of kaolinite was determined by Bish (1993) and belongs to the C1 space group. Two types of hydroxyl groups are bonded to the octahedral Al cation: (1) the inner surface hydroxyls, which interact with the siloxane groups of an adjacent layer; and (2) the inner hydroxyl O-H bonds, which are parallel to the layer. The stoichiometric ratio of these two types of kaolinite hydroxyls is 3 to 1, respectively. Consequently, the kaolinite structure is highly asymmetric, which results in strong dipolar interactions between the layers, in addition to the network of H-bonds between the inner surface hydroxyls of the aluminol groups in the octahedral sheet and the siloxane groups in the tetrahedral sheet (Giese, 1982; Detellier and Schoonheydt, 2014). These interactions between the

* E-mail address of corresponding author:
dete@uottawa.ca
DOI: 10.1346/CCMN.2017.064060

sheets of different layers result in the stacking of the layers (Mansa *et al.*, 2017), which make direct intercalation of guest molecules into the interlayer space quite challenging. Only a select group of guest compounds can directly intercalate kaolinite (Lagaly *et al.*, 2013). Because of the high dipole moment of DMSO, it can successfully intercalate kaolinite as was demonstrated by Olejnik *et al.* (1968). Later, Thompson (1985) observed two, non-equivalent ^{13}C NMR signals for the DMSO-K intercalate. Further, X-ray and neutron diffraction studies indicated that one DMSO methyl group was keyed into the ditrigonal cavity of the kaolinite layer, the other methyl group was parallel to the sheet, and the sulfonyl group was H-bonded to the aluminol sheet (Thompson and Cuff, 1985; Raupach *et al.*, 1987). When the temperature was increased above 320 K, some of the DMSO methyl groups were released from the ditrigonal cavities (Hayashi, 1997) and the interlayer DMSO that remained was H-bonded through the DMSO sulfonyl group to the aluminol groups. This behavior made DMSO-K a particularly useful and efficient starting material for the intercalation of a large variety of small molecules, polymers, and ionic liquids into kaolinite (Letaief *et al.*, 2008; Tonle *et al.*, 2009; Dedzo and Detellier, 2016). The DMSO-K in these cases functioned as a pre-intercalate material and the interlayer DMSO can be replaced by other molecular groups. An optimum DMSO replacement temperature was shown to be around 180ºC. At this temperature, the DMSO was expelled from the interlayers and simultaneously replaced by other guest compounds. At higher temperatures, the DMSO in the pre-intercalate material was completely removed before it could be replaced by other compounds and kaolinite without intercalated DMSO was recovered (Letaief and Detellier, 2011). Suitable molecular units can be simultaneously grafted to kaolinite internal surfaces at 180ºC during the intercalation process (Tonlé *et al.*, 2011; Dedzo and Detellier, 2016). An in-depth evaluation of the methods to intercalate DMSO into kaolinite was recently published (Abou-El-Sherbini *et al.*, 2017).

In addition to X-ray diffraction, infrared techniques (Johnston *et al.*, 1984; Yariv and Lapides, 2008; Scholtzova and Smrcok, 2009; Horvath *et al.*, 2010) have been extensively used in the characterization of DMSO-K. Because nuclear magnetic resonance (NMR) is a powerful tool to describe local nuclear environments, especially in the solid state, it is a useful complement to other techniques. For example, the two observed ^{29}Si MAS NMR signals confirmed the asymmetrical nature of kaolinite layers (Barron *et al.*, 1983), whereas ^{13}C MAS NMR confirmed the keyed structure of DMSO in the DMSO-K intercalate (Thompson, 1985). The use of ^{1}H and of ^{27}Al MAS NMR, however, has been much rarer, even though routine use would be very useful. The use of ^{1}H MAS NMR can give unique information on kaolinite hydroxyls and as a complementary technique to FTIR. The use of ^{1}H MAS NMR would be a particularly useful technique to follow as organic units are grafted to aluminol internal surfaces. Given the sensitivity of quadrupolar interactions on the local geometry of octahedral Al(III), solid-state ^{27}Al NMR could be very useful to follow the subtle structural modification of the octahedral sheet that follows intercalation and/or grafting. While infrared methods have been performed in several DMSO-K intercalate studies (Johnston *et al.*, 1984; Yariv and Lapides, 2008; Scholtzova and Smrcok, 2009; Horvath *et al.*, 2010), few studies have used ^{1}H NMR. The high magnetic fields combined with the use of high spinning rates allow the acquisition of high resolution ^{1}H NMR spectra in the solid state using conventional single pulse MAS NMR. Hayashi *et al.* (1992a) pioneered the use of high-resolution solid-state ^{1}H NMR to study the structure of kaolinite. They studied the static and CRAMPS (combined rotation and multiple-pulse spectroscopy) spectra for a variety of kaolinites. The CRAMPS technique is a specialized pulse program used to improve the resolution of spectra that are broadened by dipolar and shielding anisotropies in the solid state (Gerstein, 2009). In the static spectra, two components with different shapes were observed and were deconvoluted into broad and narrow components. The components were assigned to water molecules adsorbed on external kaolinite surfaces and to kaolinite structural hydroxyl groups, respectively. The ^{1}H CRAMPS NMR spectra of kaolinite gave one broad line centered at 2.8 ppm. Spin-lattice relaxation times were measured and reported in an accompanying paper (Hayashi *et al.*, 1992b). The relaxation curve was deconvoluted into two components, long and short, that were ascribed in a similar manner to external water molecules and internal hydroxyls. The spin-lattice relaxation rates obtained under MAS conditions confirmed that spin diffusion plays an important role in ^{1}H relaxation, which is diffusion-limited (Hayashi and Akiba, 1995). The ^{1}H NMR single pulse experiments were performed on two kaolinites at 300 MHz and a spinning rate of 10.5 kHz (Wang *et al.*, 2002). Two peaks for each of the two kaolinites were observed at 2.4 and −1.3 ppm and at 3.0 and −0.9 ppm, respectively. The two peaks were attributed to inner surface (2.4 and 3.0 ppm) and inner (−1.3 and −0.9 ppm) hydroxyls (Wang *et al.*, 2002). Cheng *et al.* (2015) reported the ^{1}H MAS NMR spectrum for a well ordered kaolinite. A relatively sharp signal was observed at 4.9 ppm and was attributed to inner surface hydroxyl groups, but inner hydroxyls were not observed. Zhu *et al.* (2016) obtained the ^{1}H MAS NMR spectra of three kaolinites at 500 MHz and two peaks were observed and deconvoluted. Chemical shifts in the 2.8−3.1 ppm and 1.7−1.9 ppm ranges were attributed to inner surface and inner hydroxyls, respectively. The relative populations of the chemical shifts, however, did not correspond to the expected 3:1 ratio.

In comparison to ^{1}H NMR, kaolinite ^{27}Al MAS NMR has more often been reported (Rocha and Pedrosa de Jesus, 1994; Ashbrook *et al.*, 2000; Zhou *et al.*, 2009;

https://doi.org/10.1346/CCMN.2017.064060 Published online by Cambridge University Press

Paris, 2014). Many of these studies have been focused on finding evidence for the two distinct Al sites in the kaolinite crystallographic structure that were identified in X-ray diffraction studies (Bish and Von Dreele, 1989). Small parameter differences are observed between each of the Al species, which makes distinguishing between them difficult using ^{27}Al NMR. The literature on intercalated and grafted kaolinite complexes is more limited. The published studies, however, have shown a high likelihood to observe multiple Al species, especially in grafted complexes. Tunney and Detellier (1993, 1994), for example, reported that major changes occurred to the ^{27}Al NMR spectra of kaolinite grafted with ethylene glycol. They attributed the spectral changes to ethylene glycol covalently grafted to Al in the octahedral sheets in the clay mineral structure. Hirsemann *et al*. (2011) performed multiple quantum magic-angle spinning (MQMAS) experiments on ethylene glycol grafted to kaolinite and found two Al species with different chemical shifts and quadrupolar parameters. They also performed a REAPDOR (rotational echo adiabatic passage double resonance) experiment, which allowed ethylene glycol grafted to kaolinite internal aluminol surfaces to be conclusively demonstrated. REAPDOR is a specialized pulse program used to measure the distance between spin ½ and quadrupolar nuclei in the solid state (Guillion, 1995).

The purpose of the present study was to obtain precise local structural information at the atomic level on kaolinite and on the kaolinite DMSO intercalate (DMSO-K) using ^{1}H MAS NMR spectra at 21.1 T and the ^{27}Al MAS and MQMAS NMR spectra at 21.1 and 4.7 T to (1) differentiate the inner and the inner surface hydroxyl groups, aided by partial deuteration; and (2) isolate the quadrupolar parameters of the different octahedral Al(III) sites in each of these materials by simulation of the ^{27}Al NMR spectra at low field.

MATERIALS AND METHODS

Materials

Kaolinite. The KGa-1b (Georgia) kaolinite is a highly crystalline, low defect kaolinite (Hinckley Index = 1.09) and was obtained from the Source Clays Repository of The Clay Minerals Society. It has the high purity characteristic of Georgia kaolins with anatase as the only significant impurity. The particle size distribution of KGa-1b was determined to be 57.8% <2 μm and 32.0% <0.5 μm (Pruett and Webb, 1993). A poorly crystallized kaolinite sample (KGa-2) was also used in some experiments (Figure S1 in the Supplemental Materials section (deposited with the Editor-in-Chief and available at http://www.clays.org/JOURNAL/JournalDeposits.html)). The <2 μm fraction was isolated by sedimentation using a method similar to published methods (Jeffries and Jackson, 1949). A 60-g sample of KGa-1b was dispersed in 4 L of distilled water by mechanical stirring in a beaker and the pH of the suspension was adjusted to 9.0 by the addition of 0.1 M NaOH to create a stable suspension of the clay particles. Stirring of the suspension was then stopped, the suspension was allowed to settle for 6 h, and the top two-thirds of the suspension was siphoned off and set aside. The remaining suspension was re-dispersed in distilled water and the sedimentation procedure was repeated three more times. The four siphoned suspensions were then combined and the pH was adjusted to 6.0 by the addition of 0.1 M HCl, which rapidly flocculated the clay particles. The supernatant was decanted from the suspension as much as possible without loss of solids and was discarded. The remaining kaolinite solid suspension was evenly partitioned into four 700-mL centrifugation vessels, the masses of the vessels were equalized by distilled water addition, and the vessels were centrifuged at high speed until all the solid matter was deposited. The supernatants were discarded, 300 mL of distilled water was added to the vessels, the solids were re-dispersed, and the centrifugation procedure was repeated. This distilled-water washing and centrifugation procedure was repeated two more times, the final isolated solids in the four vessels were combined together, and the solids were oven dried at 80ºC for 24 h.

Dimethyl sulfoxide - kaolinite intercalate (DMSO-K). The method used to prepare DMSO-K was similar to the one described by Olejnik *et al.* (1968). A 10-g sample of KGa-1b <2μm was dispersed in a mixture of 60 mL of DMSO and 0.1 mL of deionized water at 80ºC and allowed to equilibrate for three weeks. The resulting solid product was isolated by centrifuging at high speed until all the solid matter was deposited and the supernatant was discarded. The solid was dispersed in 200 mL of isopropanol to wash out excess DMSO and centrifuged using the same procedure described above. This procedure was repeated three times and the final solid material was oven dried at 80ºC overnight.

Deuterated kaolinite. A sample of DMSO-K (100 mg) was added to 5 mL of D_2O in a glass vial, the vial was capped, and the resulting suspension was stirred using a magnetic spin bar at room temperature for three d. The DMSO-K solid matter was isolated by centrifuging the suspension at high speed until all the solid matter was deposited and the supernatant was discarded. The solids were then transferred to an evaporation dish using 2−3 mL of acetone and oven dried at 70ºC for one h. The dried solid was then stored in a desiccator under N_2 prior to analysis.

Methods

Solid-state ^{1}H nuclear magnetic resonance. The ^{1}H MAS NMR experiments were carried out at 899.69 MHz on a 21.1 T Bruker AVANCE II NMR spectrometer using a 4 mm H/X MAS Bruker probe (Bruker BioSpin

https://doi.org/10.1346/CCMN.2017.064060 Published online by Cambridge University Press

GmbH, Rheinstetten, Germany). All experiments used an 18 kHz MAS spinning rate with a modified 90-90 rotor-sync quad-echo pulse sequence for background signal suppression. A recycle delay time (d1) of 5 s was used, which was sufficient for complete relaxation and allowed quantitative analysis of peak integrals. The chemical shift scale was referenced to the tetramethylsilane (TMS) peak at 0.0 ppm.

Solid-state ^{27}Al nuclear magnetic resonance. Lower field solid-state ^{27}Al MAS NMR spectra were obtained at 52.1 MHz on a 4.7 T Bruker AVANCE III NMR spectrometer (Bruker BioSpin GmbH, Rheinstetten, Germany) equipped with a 7 mm triple resonance MAS probe. A d1 time of 2 s was used and the solid samples were packed into a 7 mm zirconia rotor and spun at a frequency of 5 kHz. High-field ^{27}Al MAS NMR spectra were measured at 234.5 MHz on a 21.1 T Tesla Bruker AVANCE II NMR spectrometer (Bruker BioSpin GmbH, Rheinstetten, Germany) equipped with a 4 mm H/X MAS Bruker probe, using a MAS spinning rate of 18 kHz. A d1 time of 2 s was used and was sufficient for complete relaxation. In both cases, the chemical shift scale was referenced to the $^{27}Al(NO_3)_3$ peak in water at 0.0 ppm (0.5 M at 21.1 T; 0.1 M at 4.7 T). Two-dimensional ^{27}Al triple-quantum (3Q) MAS NMR experiments were performed at 21.1 T under 18 kHz MAS. All experiments were rotor-synchronized in the f1 dimension (SWH1=18 kHz, t1 increment of 55.56 μs) and employed a three-pulse z-filter 3QMAS pulse sequence. The spectral width in the direct F2 dimension was 100 kHz. For each t1 increment, 48 transients were accumulated using a 1 s relaxation delay. The total number of t1 increments was 128. The excitation and conversion pulses optimized using 60 kHz r.f. power for Al sites with small C_Q (^{27}Al) values were 5.75 μs and 1.75 μs, respectively. The ^{27}Al selective 90º pulse width was 9 μs. The chemical shift referencing in the indirect dimension was done according to the method of Millot and Man (2002).

NMR Spectral deconvolution and curve fitting. The experimental ^{1}H MAS NMR spectra were fitted with the help of the peak fitting software FityK (Wojdyr, 2010), the peak fitting was done using Voigt curves, and the rotational sidebands were not included in this analysis. This still gave an accurate fit since the vast majority of the signal intensity was in the central transition and the relative signal intensities of each peak was the same for the sidebands as it was for the central transition.

Because ^{27}Al is a quadrupolar nucleus, it produces NMR line shapes that cannot be described by classical curves and requires specialized software to simulate and fit the NMR curves. The experimental ^{27}Al MAS NMR spectra were fitted using Dmfit (Massiot *et al*., 2002), which is an NMR software package with several options for simulating the NMR spectra of quadrupolar nuclei. Fitting of the NMR spectra was done using the built in 2QUAD function, which allows the computation of spectra at static or finite MAS rates and takes into account 2nd order quadrupolar effects and chemical shift anisotropy. The central (*i.e*. CT) and satellite (*i.e*. ST1, ST2) transitions were simulated using MAS rates of 5 kHz for the 4.7 T spectra and 18 kHz for the 21.1 T spectra and 10 and 2 ppm of Gaussian line broadening, respectively.

Attenuated total reflectance Fourier-transform infrared analysis (ATR-FTIR). The ATR-FTIR spectra were obtained using a Nicolet 6700 FTIR (Thermo Scientific, 81 Wyman Street, Waltham, Massachusetts, USA) in attenuated total reflection mode using the SMART diamond ATR attachment. A background spectrum from 4500 to 650 cm^{-1} was obtained before each sample was analyzed using an average of 128 scans with a resolution of 4 cm^{-1} and the spectra were obtained with the aid of the OMNIC software package. Sample analyses were done by evenly spreading out ~2−5 mg of each solid sample and firmly pressing it to the surface of the ATR crystal. Spectra were measured using the same number of scans and spectral resolution as the background.

Powder X-ray diffraction (XRD). XRD traces were obtained using a Philips PW 3710 diffractometer (PANanalytical, Lelyweg 1, 7602 EA Almelo, The Netherlands) with a Cu $K\alpha$ radiation source (λ = 1.5406 Å), operated at 45 kV generator voltage and 40 mA current. Sample analyses were accomplished by pressing the solid materials into cylindrical pellets with a diameter of ~0.5 cm and thickness of ~2 mm and mounting the sample pellets on disk shaped sample holders.

Thermal gravimetric analysis (TGA). TGA mass loss curves were obtained using a Q500 Thermal Gravimetric Analyzer (TA Instruments, New Castle, Delaware, USA). Sample solids (2−5 mg) were loaded into a 50 μL tared high temperature Pt pan and analyzed using a steady temperature ramp program of 10ºC min^{-1} under a N_2 flow rate of 25 mL min^{-1}. A one min isothermal temperature hold was done at the beginning of each experiment to allow the movements of the sample pan to stabilize after it was loaded inside the furnace.

CHNS Elemental analysis. Elemental analyses were performed at the G.G. Hatch Stable Isotope Laboratory of the University of Ottawa. The standard protocol employed for elemental analysis has a routine analytical precision of ±0.1% and is summarized as follows: (1) samples and standards were weighed into Sn capsules and loaded into an Elementar Isotope Cube elemental analyzer (Elementar, Langenselbold, Germany); (2) the Sn sample capsules were flash

https://doi.org/10.1346/CCMN.2017.064060 Published online by Cambridge University Press

combusted in the analyzer at about 1800ºC in O_2 carried by a He flow through columns of reducing/oxidizing chemicals to produce N_2, CO_2, and SO_2; and (3) the N_2, CO_2, and SO_2 gases were separated in a trap and purge system of adsorption columns to separately measure each gas using the thermal conductivity detector.

RESULTS AND DISCUSSION

The ^{1}H MAS NMR spectrum of the <2 μm KGa-1b sample was obtained at 900 MHz (Figure 1) and the spectrum was consistent with previously reported results (Wang *et al*., 2002; Zhu *et al*., 2016). Two overlapping, but distinctly different, signals in the 1 to 3 ppm range with a broad shoulder at higher chemical shifts were observed. The spectrum was deconvoluted using Voigt curves. The Voigt function is a combination of Cauchy (*i.e*. Lorentzian) and Gaussian functions and is commonly used for curve fitting in spectroscopy and crystallography due to the wide variety of line shapes it can simulate (Armstrong, 1967; Langford, 1978). Whereas the Fourier transformation of the free induction decay plot in NMR is expected to give a purely Lorentzian line shape, the line broadening effect from dipolar interactions will produce a Gaussian convolution in the solid state (Van Vleck, 1948; Kittel and Abrahams, 1953). Consequently, a function which combines both line shapes is commonly used to obtain an accurate deconvolution of the observed signal. The deconvolution result is also given in Figure 1. Two major signals at 1.70 and 2.68 ppm were measured with relative intensities of 1.00 and 3.09. This result is consistent with the expected proton site ratio in the clay mineral, where 1 out of every 4 hydroxyls in the idealized $Al_2Si_2O_5(OH)_4$ kaolinite structure is an inner hydroxyl and the other 3 hydroxyls are inner surface hydroxyls. As a result, the ratio of the integrated signal of the inner surface hydroxyl protons to the integrated signal of inner hydroxyl protons should be 3:1, which is in close agreement with the experimental ratios. Consequently, the 1.70 ppm signal was attributed to the inner hydroxyl, while the 2.68 ppm signal was attributed to the inner surface hydroxyls. One should also note that the best fits to the experimental spectra were obtained when the inner surface hydroxyl peak at 2.68 ppm was broader and had a more Gaussian character than the inner hydroxyl peak signal at 1.70 ppm. This further supports the signal assignments. The inner hydroxyls are segregated from the other hydroxyl groups, but the inner surface hydroxyls are close to other hydroxyl groups and experience more ^{1}H-^{1}H dipolar interactions. This should result in a more Gaussian line shape. In addition, one should expect a larger chemical shift dispersion from the inner surface hydroxyls than from the inner hydroxyls. These observed ^{1}H chemical shift values are in good agreement with reported chemical shifts of ~0.5 ppm for trioctahedral smectite internal hydroxyl groups and ~2.0 ppm for dioctahedral smectites (Alba *et al*., 2000). In dioctahedral sheets, the internal OH bonds are almost parallel to the layers and allow an H-bond with the apical oxygen atoms of the tetrahedral sheet, which results in decreased chemical shielding. In trioctahedral sheets, the internal OH bonds are perpendicular to the layers and point

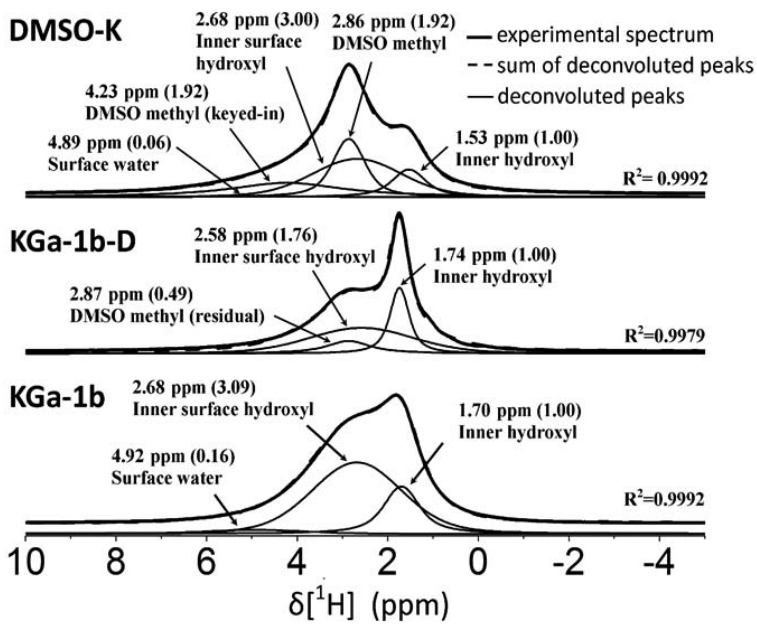

Figure 1. ^{1}H MAS NMR of KGa-1b, KGa-1b-D, and DMSO-K and curve fitting results. The relative signal ratios are shown in parentheses.

https://doi.org/10.1346/CCMN.2017.064060 Published online by Cambridge University Press

toward the hexagonal cavities, which is not favorable for strong H-bonds.

Wang *et al.* (2002) reported chemical shift values of 2.4 and −1.3 ppm for one kaolinite and 3.0 and −0.9 ppm for another kaolinite. These values were attributed to inner surface (2.4 and 3.0 ppm) and inner (−1.3 and −0.9 ppm) hydroxyls. The negative chemical shifts were surprising and are closer to what was expected for a trioctahedral sheet than for a dioctahedral sheet. In addition, Wang *et al.* (2002) reported relative peak intensities for the inner surface and inner hydroxyls of 62% and 38% for one kaolinite and 27% and 73% for the other kaolinite. This significantly deviated from the expected 3:1 relative intensity ratio. Two ^{1}H NMR peaks were observed and deconvoluted by Zhu *et al.* (2016), with chemical shifts in the 2.8−3.1 ppm and 1.7−1.9 ppm ranges that were attributed to inner surface and inner hydroxyls, respectively. The Zhu *et al.* (2016) relative peak intensities also did not have the expected 3:1 ratio and the chemical shift values were close to those observed in the present study. In only one case was the measured relative hydroxyl population ratio (3.3:1) fairly close to the expected 3:1 structural value and the ratios were 2:3 in the other two cases. The discrepancy between measured and expected hydroxyl populations was attributed to different degrees of bond rupture on kaolinite platelet edges where the inner hydroxyls are exposed to give a similar environment to the inner surface hydroxyls. This argument was difficult to follow using the published FESEM images, which indicated particle dimensions in the 0.5−1 μm range and consequently a very small percentage of edge hydroxyls (Zhu *et al.*, 2016). To account for the broad shoulder in the ^{1}H MAS NMR spectrum at higher frequencies in the present work (Figure 1), the deconvolution included a third weak and broad signal centered at 4.92 ppm. This resonance was attributed to surface water present in the material. TGA weight loss analysis of the sample indicated that 0.46 % (w/w) water was present in the kaolinite under study. This quantity of water would give a proton abundance of 0.13 relative to the inner hydroxyls. Using this abundance, a best fit to the experimental spectrum was obtained when this peak was centered at 4.92 ppm. This value was expected to depend greatly on the amount of water adsorbed on the external surfaces (Li *et al.*, 2010; Zhu *et al.*, 2016).

To further confirm the signal attributions in the ^{1}H MAS NMR spectra, an attempt was made to deuterate the KGa-1b by washing the DMSO-K intercalate with deuterated water (see Materials and Methods). The D_2O intercalation process should remove DMSO and leave unexpanded kaolinite with deuterated inner surface hydroxyls. This allows the inner surface hydroxyls to be differentiated from the inner hydroxyls, which are known to be much more resistant to deuteration (Ledoux and White, 1964). Deuterium exchange, thus, could be an effective way to identify the inner hydroxyl groups in kaolinite. In addition, this would also be expected to have a line narrowing effect due to a reduction in dipolar interactions. The attempt to deuterate directly KGa-1b by washing with D_2O repeatedly at room temperature was, as expected, unsuccessful. This is clearly because hydroxyl groups in natural kaolinite exchange with deuterium only under high temperature and pressure (Romo, 1956). Even under high temperature and pressure conditions, however, the inner hydroxyls are exchanged with difficulty. FTIR spectra of KGa-1b and deuterated kaolinite in the region expected for the O-D stretching bonds are shown in Figure 2. The absorption frequency that corresponds to the KGa-1b inner hydroxyl was observed at 3620 cm^{-1} (Johnston *et al.*, 1990). The deuterated KGa-1b inner hydroxyl was observed at 2676 cm^{-1} and had an intensity that was strongly reduced in comparison to the other character-

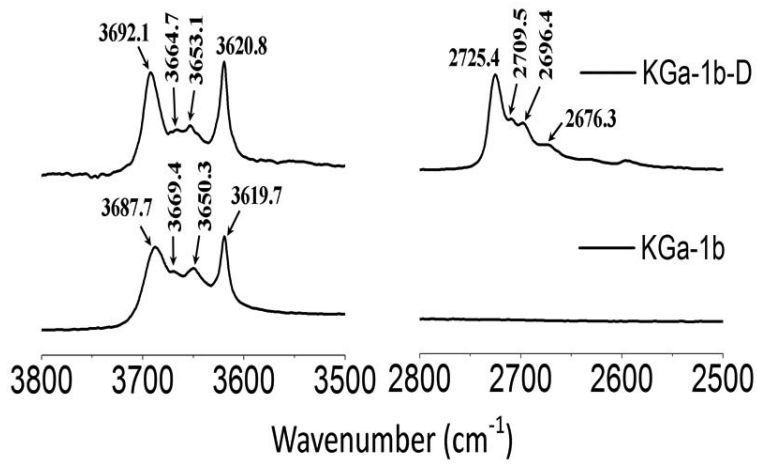

Figure 2. ATR-FTIR spectrum of KGa-1b and deuterated KGa-1b (KGa-1b-D). Close-ups of the 3800–3500 and 2800–2500 cm^{-1} regions are shown.

https://doi.org/10.1346/CCMN.2017.064060 Published online by Cambridge University Press

istic absorption frequencies of kaolinite. This was because the inner surface hydroxyls are much more accessible than the inner hydroxyls, which resulted in selective deuteration. Similarly, Johansson *et al.* (1998) found that the vibrational frequency ν_H was not exactly 1.37 times ν_D as predicted by Hooke's law, but rather was 1.35 and likely resulted from an isotopic effect on the O-H/O-D bond strengths. Consequently, the ^{1}H MAS NMR spectrum of deuterated kaolinite, KGa-1b-D, should confirm the attribution of the 1.70 ppm signal to the inner hydroxyls because this peak should have become more intense in comparison to the 2.68 ppm signal that was attributed to the inner surface hydroxyls. This is exactly what was observed experimentally (Figure 1). The ^{1}H MAS NMR spectrum of deuterated KGa-1b-D (Figure 1) appeared very different from the initial KGa-1b sample. The deconvolution gave two main signals at 1.74 ppm and 2.58 ppm, which were similar to the spectrum of KGa-1b but with different ratios. The 1.74 and 2.58 ppm signals were, respectively, attributed to the inner hydroxyls and to the inner surface hydroxyls. In comparison to the KGa-1b spectrum, the 2.58 ppm signal population was reduced by almost a factor of two in the KGa-1b-D spectrum, which resulted from the more efficient deuteration of the inner surface hydroxyls. Additionally, the signal from surface adsorbed water disappeared. The new broad signal at 2.87 ppm was attributed to residual DMSO molecules and the DMSO contents determined from TGA, and CHNS elemental analysis were 0.022 and 0.025 moles/100 g, respectively. Deconvolution of the ^{1}H MAS NMR signal indicated a similar DMSO content of 0.032 moles/100 g of material. One should note that only one signal was sufficient to account for the small amounts of DMSO. This contrasts with the deconvolution of DMSO-K signals which was based on two signals of equal intensity for DMSO (see below). The use of two DMSO signals with a ^{1}H population of 0.49/2 each and chemical shifts provided by the DMSO-K spectrum did not improve the deconvolution. As mentioned above, several previous reports demonstrated that one of the two DMSO methyl groups in DMSO-K was keyed into the kaolinite siloxane ring of the tetrahedral sheet, while the other methyl group was parallel to the layer (Johnston *et al*., 1984, Thompson, 1985; Duer *et al.*, 1992; Duer and Rocha, 1992; Hayashi, 1997). The ^{13}C MAS NMR spectrum of DMSO-K was recorded and two signals were observed at 44.2 and 43.1 ppm, which is in agreement with this structure. Consequently, to analyze the ^{1}H NMR spectrum of DMSO-K, a model to take this fact into consideration was used. The ^{1}H NMR spectrum of DMSO-K and a deconvolution of the spectrum into several components (Figure 1) included the two kaolinite hydroxyl signals with respective intensities of 1 and 3 and two DMSO methyl signals of equal intensity. A small amount of water confirmed by TGA had a molar fraction of 0.03 and was included in the deconvolution as a broad and low intensity band at 4.89 ppm. The best fit was obtained when the chemical shift of the keyed-in methyl group of DMSO was 4.23 ppm, while the other methyl group was observed at 2.86 ppm.

The ^{27}Al MAS NMR spectra were recorded for KGa-1b at two different magnetic fields of 21.1 T and 4.7 T (Figure 3). The signal maxima were observed, respectively, at 6.4 ppm and −18.2 ppm and had noticeable differences in the line shapes. The quadrupolar effects were minimized at 21.1 T, but strongly affected the signal at 4.7 T. The signal observed at 6.4 ppm was consistent with a six-coordinated Al(III), which is expected to give a signal between −10 to +15 ppm (Mackenzie and Smith, 2002). The 6.4 ppm value at 21.1 T should be close to the true isotropic chemical shift, δ_{iso}, because the signal center of gravity is proportional to the inverse square of the applied magnetic field (MacKenzie and Smith, 2002; Wasylishen *et al*., 2012). An extrapolation to $B_0^{-2} = 0$ for the spectra centers of gravity at 4.7 T and 21.1 T gave a δ_{iso} value of 8.3 ppm. Close examination of the 21.1 T spectrum (Figure 3) revealed that the central peak (CT) base is not symmetrical and the line shape is distorted at higher frequencies. This was attributed to the presence of the satellite transitions, ST1 and ST2, which respectively resulted from the spin transitions of ±1/2 → ±3/2 and ±3/2 → ±5/2. This is more obvious in the spinning side band structure (Figure 4). In the first spinning side band (ssb) pairs, the CT transition signal dropped dramatically, but the ST transition intensities dropped to a much lesser degree such that the transitions became clearly resolved from the CT. Trace amounts of tetrahedral ^{IV}Al(III) were also observed in the close-up of the spectrum (Figure 4). This peak was centered at 71.0 ppm, which is consistent with a four-coordinated Al-O species that was expected to give a signal between

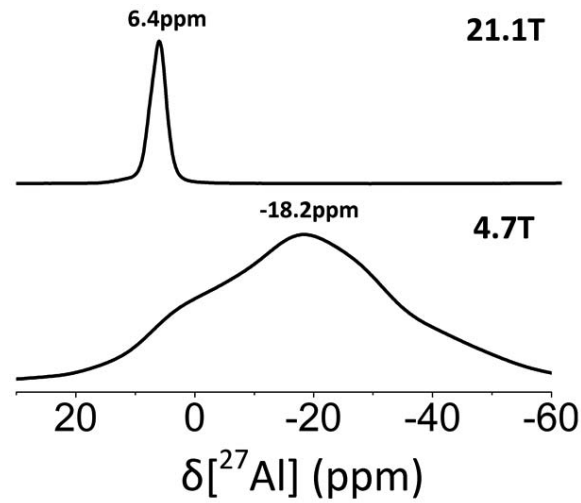

Figure 3. ^{27}Al MAS NMR spectra of KGa-1b obtained under magnetic fields of 21.1 T and 4.7 T.

https://doi.org/10.1346/CCMN.2017.064060 Published online by Cambridge University Press

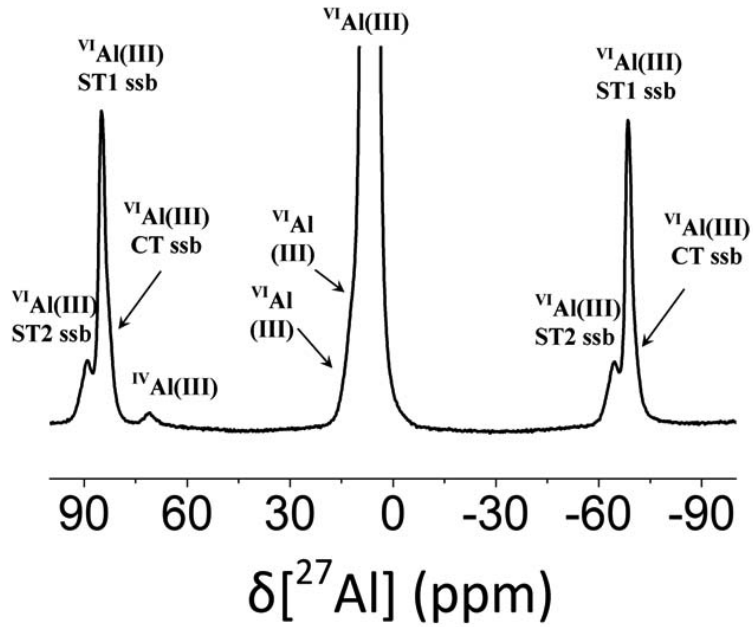

Figure 4. ^{27}Al MAS NMR spectrum of KGa-1b at 21.1 T and 18 kHz MAS, showing the line shape of the first spinning sideband pair.

50 and 80 ppm (Mackenzie and Smith, 2002) and plausibly resulted from Al substitution for Si in the tetrahedral sheet. If multiple sites for the Al(III) cation in the kaolinite structure existed, the sites could not be identified from the spectrum at very high field due to the very similar isotropic chemical shifts. On the other hand, if the quadrupolar coupling constant, C_Q, and/or the asymmetry parameter, η_Q, were sufficiently different, a low magnetic field might be used to maximize the quadrupolar effects on the NMR spectra. This would result in the detection of separate and crystallographically different Al(III) cationic sites even if the chemical shifts were similar or even identical. The ^{27}Al MAS NMR spectrum of KGa-1b was recorded at 4.7 T and the central peak position was significantly shifted towards lower frequencies with a maximum at −18.2 ppm (Figure 3). A number of features were observed on both sides of the peaks, which resulted from the increased quadrupolar effects at lower field strengths. Line shapes were simulated using models for one and for two Al(III) sites (Figure S2 in Supplemental Materials section, Figure 5). Using the δ_{iso} value found by extrapolation at infinite magnetic field strength, the best fit in the case of one site was found using C_Q = 3.21 MHz and η_Q = 0.75 values when fitted to the 4.7 T experimental spectrum. This gave a reasonable fit overall, but the line shape did not match well with the experimental line shape on the lower frequency side (Figure S2 in Supplemental Materials section), suggesting that at least another Al site was present. Simulation was then repeated by assuming two unique Al sites of equal intensity. Fitting this model to the 4.7 T experimental spectrum gave an improvement in comparison to the one-site model. This fit (Figure 5) and the parameters extracted from it (Table 1) were then successfully used to fit the spectrum obtained at 21.1 T. The deconvolution values were very close to the values that Paris (2014) reported for kaolinite and were in agreement with other previously reported values (Hayashi *et al*., 1992a; Rocha and Pedrosa de Jesus, 1994; Crosson *et al*., 2006; Zhou *et al*., 2009) as discussed by Paris (2014). This described approach was consequently validated and could be applied to other systems.

The ^{27}Al MAS NMR spectrum of DMSO-K recorded at 21.1 T (Figure 6) was compared to the corresponding

Table 1. Kaolinite ^{27}Al MAS NMR parameters for KGa-1b identified by fitting the 4.7 T and 21.1 T experimental spectra.

	δ_{iso} (ppm)	C_Q (MHz)	η_Q	Rel. abundance
Site 1	7.8 (8.0)[a]	2.9 (3.0)[a]	0.92 (0.9)[a]	0.50
Site 2	7.7 (7.5)[a]	3.4 (3.4)[a]	0.78 (0.8)[a]	0.50

[a] (Paris, 2014)

https://doi.org/10.1346/CCMN.2017.064060 Published online by Cambridge University Press

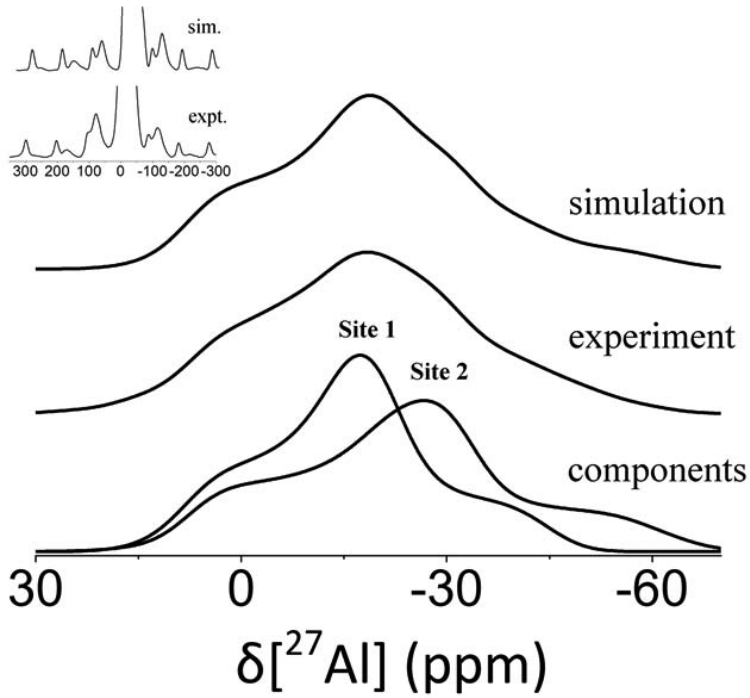

Figure 5. ^{27}Al MAS NMR spectra of KGa-1b at 4.7 T fitted to a simulated spectrum using two unique Al sites. A close up of the side bands is shown as an inset. The chemical shift value and quadrupolar parameters of each site are summarized in Table 1.

spectra of KGa-1b and KGa-1b-D at the same field. The KGa-1b and KGa-1b-D spectra were almost identical despite the small amount of DMSO that remained trapped in KGa-1b-D, which confirms the successful deuteration of the inner surface hydroxyls of kaolinite. The ^{27}Al MAS NMR spectrum of DMSO-K showed subtle line-shape changes compared to KGa-1b. A shift in the central peak maximum from 6.4 to 5.8 ppm was also observed, which occurred only on the lower frequency side of the peak. This may indicate that the shift was due to changes in the quadrupolar interaction (*i.e.* C_Q) rather than in the isotropic chemical shift (δ_{iso}) of the Al species.

To verify this, the spectrum was recorded at 4.7 T in order to amplify the quadrupolar effects and compared to the KGa-1b spectrum (Figure 7). Similar to the 21.1 T case, a shift towards lower frequency was observed, but the shift was much more dramatic at low magnetic field

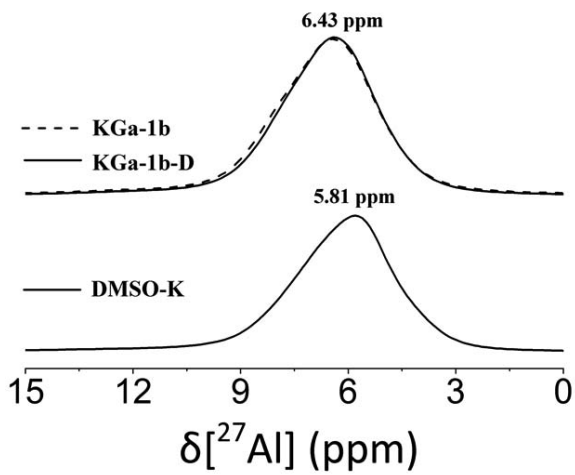

Figure 6. ^{27}Al MAS NMR spectra of DMSO-K compared to KGa-1b and KGa-1b-D. These spectra were obtained at 21.1 T using a MAS rate of 18 kHz. The removal of 88% of interlayer DMSO resulted in a line shape of KGa-1b-D almost identical to the one of KGa-1b.

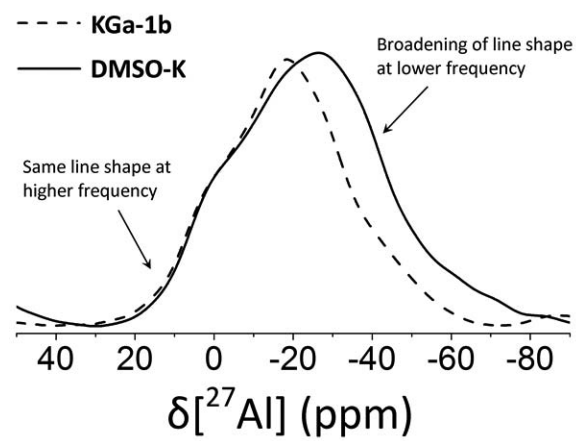

Figure 7. Superposition of the experimental ^{27}Al MAS NMR spectra of KGa-1b and DMSO-K recorded at 4.7 T. The broadening towards lower frequency in DMSO-K was likely due to higher values of C_Q (see text).

https://doi.org/10.1346/CCMN.2017.064060 Published online by Cambridge University Press

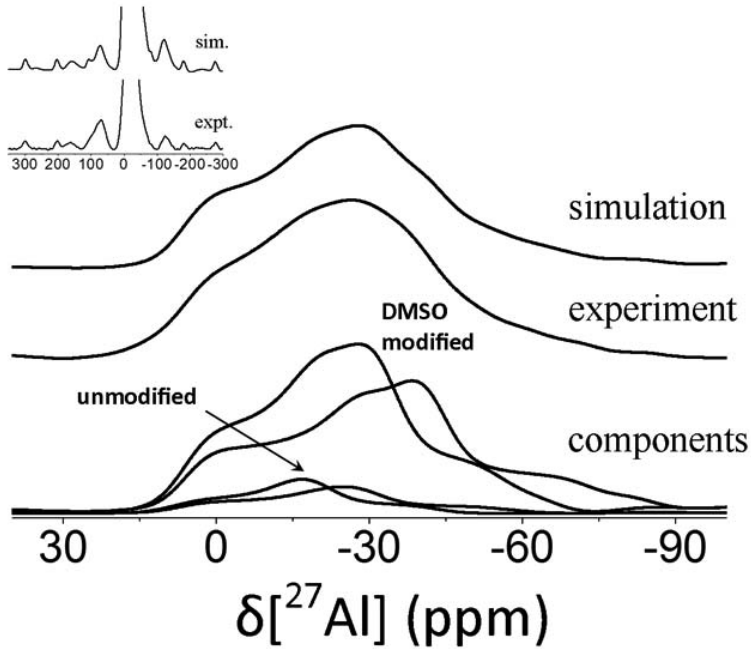

Figure 8. ^{27}Al MAS NMR spectra of DMSO-K recorded at 4.7 T fitted to a simulated spectrum using two unique Al sites each for the DMSO modified and unmodified kaolinite phases. A close up of the side bands is shown as an inset. The chemical shift value and quadrupolar parameters of each site are summarized in Table 2.

strength and the DMSO-K central peak maximum was observed at −26.4 ppm. The superposition of this spectrum with KGa-1b showed that this shift occurred on the lower frequency side of the signal, which is strong evidence that it resulted from changes in quadrupolar parameters rather than in δ_{iso}. This is because the 2nd order quadrupolar interaction with the chemical shift is negative. At higher magnetic fields, these 2nd order effects were reduced and gave a central transition that is fairly symmetric at a position close to δ_{iso}. Spectra obtained at lower field, on the other hand, exhibited much stronger 2nd order effects, which caused the central peak to broaden towards more negative frequencies (Mackenzie and Smith, 2002). At a low magnetic field, the details of the central peak became much more apparent. From the shape of the signal, a superposition of the Al sites was apparent with some sites that had parameters identical to KGa-1b and some sites that had an increased C_Q value. The 4.7 T spectrum was simulated by assuming that the DMSO molecule coverage of internal kaolinite surfaces was complete in the 11Å XRD phase and accounted for the 88% intercalation ratio revealed by XRD. The 12% abundance of the unmodified kaolinite phase was taken into account and gave relative abundances of 0.44:0.44 and 0.06:0.06 for the two DMSO-K Al sites and the two KGa-1b Al sites, respectively (Figure 8 and Table 2). One should note that a 3-site model with only one DMSO-K Al site gave an unsatisfactory fit to the experimental spectrum. The DMSO intercalation of KGa-1b resulted in a pronounced increase in the quadrupolar coupling constant, C_Q, for both Al sites and reduced the asymmetry parameter, whereas the chemical shifts were mostly unchanged. These results pointed to a distortion in the Al octahedron that resulted from interactions of intercalated DMSO through the aluminol groups. The value of C_Q (^{27}Al) depends on the Al-O bond length and on the O-Al-O bond angle (Ghose and Tsang, 1973; MacKenzie and Smith, 2002). Interactions between the interlayer DMSO sulfoxide groups and Al-OH groups in the clay mineral

Table 2. Kaolinite ^{27}Al MAS NMR parameters for DMSO intercalated KGa-1b (DMSO-K) identified by fitting the 4.7 T and 21.1 T experimental spectra.

	δ_{iso} (ppm)	C_Q (MHz)	η_Q	Rel. abundance
Site 1, modified phase	7.5	3.5	0.67	0.44
Site 2, modified phase	7.4	3.9	0.70	0.44
Site 1, unmodified phase	7.8	2.9	0.92	0.06
Site 2, unmodified phase	7.7	3.4	0.78	0.06

https://doi.org/10.1346/CCMN.2017.064060 Published online by Cambridge University Press

octahedral sheet distorted the Al-O octahedron and resulted in an increase in the C_Q value. The keyed-in methyl structure adopted by DMSO with the tetrahedral sheet should also distort the Si-O groups, which could result in additional distortion in the octahedral sheet through the shared oxygen atoms. Crystallographic data on Al octahedra in kaolinite DMSO intercalates is rather limited; so, even though the position of DMSO in the clay mineral has been well established (Hayashi, 1997), descriptions of the changes that occur in Al-O groups from interlayer DMSO are more scarce. Raupach *et al*. (1987) did report slight differences in the horizontal *ab* plane for their refined structures of DMSO-K intercalates, which they attributed to distortions in individual kaolinite layers as a result of intercalated DMSO. Simulation studies have also shown similar results (Michalková and Tunega, 2007). Infrared studies further revealed that hydrogen bonding interactions that occur between internal surface hydroxyls and interlayer DMSO molecules result in new OH stretching bands in kaolinite DMSO intercalates (Johnston *et al*., 1984; Frost *et al*., 1998). These results support the model of a more distorted Al octahedron as a result of interlayer hydrogen bonding, which produces a greater C_Q value.

Two-dimensional multiple-quantum (MQ) ^{27}Al MAS NMR spectra are often recorded to resolve overlapping Al sites and is aided by the fact that the quadrupolar broadening effects are attenuated in these spectra in the indirect (f1) multi-quantum dimension. Triple-quantum (3QMAS) ^{27}Al NMR spectra in KGa-1b and DMSO-K samples were acquired at 21.1 T (Figure 9). Because ^{27}Al NMR parameters of the two KGa-1b Al sites are very similar and overlap strongly at such high magnetic fields, the individual Al sites cannot be resolved by these ^{27}Al 3QMAS NMR spectra. Comparison of apparent differences, however, between the ^{27}Al 3QMAS NMR spectra of KGa-1b and DMSO-K (Figures 9a, 9b) clearly revealed that the effective (averaged over two Al sites) isotropic chemical shifts in the two samples are nearly identical within the experimental errors of +8.0 ppm in KGa-1b and +7.5 ppm in DMSO-K. At the same time, the second order quadrupolar effect (SOQE), which is a combined function of C_Q and η_Q, is noticeably larger in DMSO-K (4.1 MHz) in comparison to KGa-1b (3.8 MHz) and this is in agreement with the analysis and results of the one-dimensional MAS experiments.

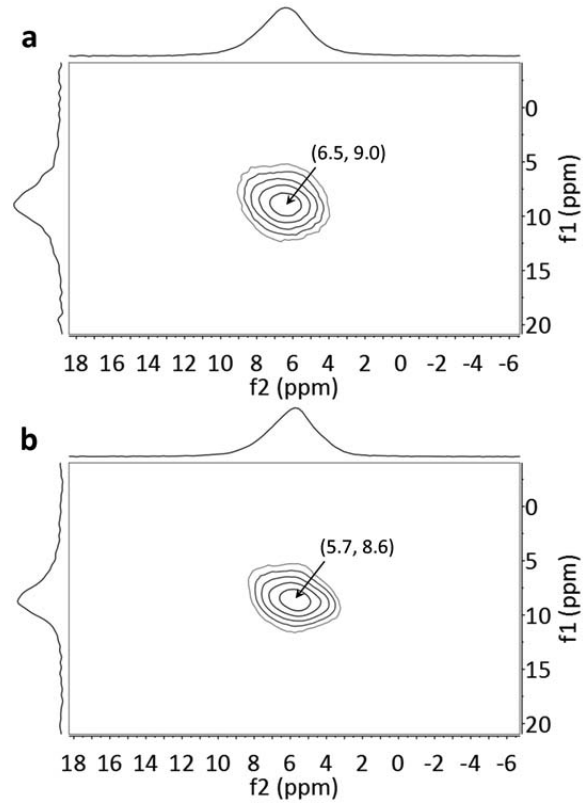

Figure 9. ^{27}Al 3QMAS NMR spectra of (a) KGa-1b and (b) DMSO-K obtained at 21.1 T using a MAS rate of 18 kHz. The peak positions in the two dimensions (f_2, f_1) were identified using the automated MestReNova software peak picking tool.

CONCLUSIONS

The ^{1}H MAS NMR chemical shifts observed in the highly crystalline, low defect, Georgia kaolinite, KGa-1b, were unambiguously attributed to the internal surface hydroxyls at 2.7 ppm and to the internal hydroxyls at 1.7 ppm. The ratio of the internal surface and the internal hydroxyl intensities was 3:1 as expected from the kaolinite structure. Kaolinite was partially deuterated by exchanging the hydroxyl protons in a kaolinite expanded with DMSO molecules with deuterated water. After deuterated water treatment, the 3:1 ratio dropped to 1.8:1 as the result of partial deuteration of the internal surface hydroxyls. This is in agreement with the signal attribution and with the observed O-D stretching region of the FTIR spectrum. The ^{1}H MAS NMR chemical shifts of the DMSO intercalate, DMSO-K, were obtained by deconvoluting the spectra into four major signals. Two signals with a 3:1 ratio were attributed to the kaolinite hydroxyls and two signals were attributed to the two non-equivalent DMSO methyl groups with identical intensities at 2.9 and 4.2 ppm. The ^{27}Al MAS NMR spectra of KGa-1b were obtained at 21.1 T and at 4.7 T. Most of the quadrupolar effects were highly reduced at 21.1 T where the signal shape mainly resulted from chemical shift dispersion effects and the low field spectra were dominated by quadrupolar effects. The two non-equivalent octahedral Al(III) sites were identified by simulating the low-field spectra. Because the isotropic chemical shifts were very similar, the shifts were differentiated by analyzing the line shape to determine the quadrupolar coupling constants and the asymmetry parameters. The quadrupolar coupling constants and asymmetry parameters, which are much more sensitive to local

https://doi.org/10.1346/CCMN.2017.064060 Published online by Cambridge University Press

symmetry perturbations in comparison to the isotropic chemical shifts, and the ^{27}Al NMR isotropic chemical shifts of 7.7 and 7.8 ppm were generally in good agreement with previously reported values. The ^{27}Al NMR values obtained for kaolinite allowed the simulation of the DMSO intercalate ^{27}Al NMR spectrum using four signals, which used two sites for the 12% non-intercalated kaolinite and two sites for the 88% intercalated kaolinite. The quadrupolar constants notably increased and the asymmetry parameters decreased after DMSO intercalation and showed that the major perturbation effect on the local Al symmetry resulted from DMSO intercalation and the rigid structural effect on the interlayer space. Finally, multiple quantum ^{27}Al MAS NMR spectra of KGa-1b and DMSO-K were recorded at 21.1 T and indicated that line-shape variations between KGa-1b and DMSO-K observed in the ^{27}Al MAS NMR spectra resulted from changes in quadrupolar parameters rather than changes in the δ_{iso} values. Both ^{1}H and ^{27}Al MAS NMR studies at several different magnetic fields have the potential to reveal important information about the local environment of kaolinite hydroxyl groups and structural Al(III), which could prove an essential complement to other techniques.

ACKNOWLEDGMENTS

The Natural Sciences and Engineering Research Council of Canada (NSERC) is gratefully acknowledged for a Discovery Grant to CD. The Canada Foundation for Innovation and the Ontario Research Fund are gratefully acknowledged for infrastructure grants to the Center for Catalysis Research and Innovation of the University of Ottawa. Access to the 21.1 T NMR spectrometer was provided by the National Ultrahigh-Field NMR Facility for Solids (Ottawa, Canada), a national research facility funded by a consortium of Canadian Universities supported by the National Research Council Canada and Bruker BioSpin and managed by the University of Ottawa (http://nmr900.ca). The staff at the G.G. Hatch Stable Isotope Laboratory (University of Ottawa, Canada) are thanked for performing the CHNS elemental analysis. Dr Glenn Facey of the University of Ottawa is gratefully thanked for his help in recording the NMR spectra at lower fields.

REFERENCES

Abou-El-Sherbini, K.S., Elzahany, E.A.M., Wahba, M.A., Drweesh, S.A., and Youssef, N.S. (2017) Evaluation of some intercalation methods of dimethylsulfoxide onto HCl-treated and untreated Egyptian kaolinite. *Applied Clay Science*, **137**, 33–42.

Alba, M.D., Becerro, A.I., Castro, M.A., and Perdigón, A.C. (2000) High-resolution ^{1}H MAS NMR spectra of 2:1 phyllosilicates. *Chemical Communications*, 37–38.

Armstrong, B.H. (1967) Spectrum line profiles: the Voigt function. *Journal of Quantitative Spectroscopy and Radiative Transfer*, **7**, 61–88.

Ashbrook, S.E., McManus, J., MacKenzie, K.J.D., and Wimperis, S. (2000) Multiple-quantum and cross-polarized ^{27}Al MAS NMR of mechanically treated mixtures of kaolinite and gibbsite. *Journal of Physical Chemistry B*, **104**, 6408–6416.

Bish, D.L. and Von Dreele, R.B. (1989) Rietveld refinement of non-hydrogen atomic positions in kaolinite. *Clays and Clay Minerals*, **37**, 289–296.

Bish, D.L. (1993) Rietveld refinement of the kaolinite structure at 1.5K. *Clays and Clay Minerals*, **41**, 738–744.

Barron, P.F., Frost, R.L., and Skjemstad, J.O. (1983) Detection of two silicon environments in kaolins via solid-state ^{29}Si NMR. *Nature*, **302**, 49–50.

Bergaya, F. and Lagaly, G. (2013) General Introduction: Clays, Clay Minerals, and Clay Science. Chapter 1, pp. 1–19, in: *Handbook of Clay Science* (F. Bergaya and G. Lagaly, editors). Developments in Clay Science. Vol. **5**, 2nd ed. Elsevier, Amsterdam.

Brack, A. (2013) Clay minerals and the origin of life. Chapter 10, pp. 507–522 in: *Handbook of Clay Science* (F. Bergaya and G. Lagaly, editors). Developments in Clay Science, Vol. **5**, *2nd* ed. Part A. Elsevier, Amsterdam.

Brigatti, M.F., Galán, E., and Theng, B.K.G. (2013) Structure and mineralogy of clay minerals. pp. 29–35 in: *Handbook of Clay Science* (F. Bergaya and G. Lagaly, editors). Developments in Clay Science. Vol. **5**, 2nd ed. Part A, Elsevier, Amsterdam

Cheng, H., Hou, X., Liu, Q., Li, X., and Frost R.L. (2015) New insights into the molecular structure of kaolinite – methanol intercalation complexes. *Applied Clay Science*, **109-110**, 55–63.

Crosson, G.S., Choi, S.Y., Chorover, J., Amistadi, M.K. O'Day, P.A., and Mueller, K.T. (2006) Solid-state NMR identification and quantification of newly formed aluminosilicate phases in weathered kaolinite systems. *Journal of Physical Chemistry B*, **110**, 723–732.

Dedzo, G.K. and Detellier, C. (2016) Functional nanohybrid materials derived from kaolinite. *Applied Clay Science*, **130**, 33–39.

Detellier, C. and Schoonheydt, R.A. (2014) From Platy Kaolinite to Nanorolls. *Elements*, **10**, 201–206.

Detellier, C., Letaief, S., Fafard, J., and Dedzo, G.K. (2015) Desorption of bitumen from clay particles and mature fine tailings, US Patent application No 14/083,824; US 2015/0136651 A1: published May 21, 2015.

Duer, M.J., Rocha, J., and Klinowski, J. (1992) Solid-state NMR studies of the molecular motion in the kaolinite:DMSO intercalate. *Journal of the American Chemical Society*, **114**, 6867–6874.

Duer, M.J. and Rocha, J. (1992) A two-dimensional solid-state exchange NMR study of the molecular motion in the kaolinite: DMSO intercalation compound. *Journal of Magnetic Resonance*, **98**, 524–533.

Frost, R.L., Kristof, J., Paroz, G.N., and Kloprogge, J.T. (1998) Molecular structure of dimethyl sulfoxide intercalated kaolinites. *The Journal of Physical Chemistry B*, **102**, 8519–8532.

Galimberti, M., Cipolletti, V.R., and Coombs, M. (2013) Applications of clay-polymer nanocomposites. Pp. 539–586. Chapter 4 in: *Handbook of Clay Science* (F. Bergaya and G. Lagaly, editors), Developments in Clay Science, Vol. **5B**, 2nd edition, Elsevier, Amsterdam.

Gerstein, B.C. (2009) *CRAMPS: High-Resolution NMR of High-γ Nuclei in Solids*. eMagRes. Wiley Online Library, DOI: 10.1002/9780470034590.emrstm0100. pub2. J. Wiley & Sons, Inc.

Ghose, S. and Tsang, T. (1973) Structural Dependence of Quadrupole Coupling Constant e^2qQ/h for ^{27}Al and Crystal Field Parameter D for Fe^{3+} in Aluminosilicates. *American Mineralogist*, **58**, 748–755.

Giese, R.F. (1982) Theoretical studies of the kaolin minerals – electrostatic calculations. *Bulletin de Minéralogie*, **105**, 417–424.

Gullion, T. (1995) Measurement of dipolar interactions

between spin-1/2 and quadrupolar nuclei by rotational-echo, adiabatic-passage, double-resonance NMR. *Chemical Physics Letters*, **246**, 325–330.

Hayashi, S., Ueda, T., Hayamizu, K., and Akiba, E. (1992a) NMR study of kaolinite. 1. ^{29}Si, ^{27}Al, and ^{1}H spectra. *Journal of Physical Chemistry*, **96**, 10922–10928.

Hayashi, S., Ueda, T., Hayamizu, K., and Akiba, E. (1992b) NMR study of kaolinite. 2. ^{1}H, ^{27}Al, and ^{29}Si spin-lattice relaxations. *Journal of Physical Chemistry*, **96**, 10928–10933.

Hayashi, S. and Akiba, E. (1995) Nuclear spin-lattice relaxation mechanisms in kaolinite confirmed by magic-angle spinning. *Solid State Nuclear Magnetic Resonance*, **4**, 331–340.

Hayashi, S. (1997) NMR study of dynamics and evolution of guest molecules in kaolinite /dimethylsulfoxide intercalation compound. *Clays and Clay Minerals*, **45**, 724–732.

Hirsemann, D., Köster, T.K.-J., Wack, J., van Wüllen, L., Breu, J., and Senker, J. (2011) Covalent grafting to μ-hydroxy-capped surfaces? A kaolinite case study. *Chemistry of Materials*, **23**, 3152–3158.

Horvath, E., Kristof, J., and Frost, R.L. (2010) Vibrational spectroscopy of intercalated kaolinite. Part I. *Applied Spectroscopy Reviews*, **45**, 130–147.

Jeffries, C.D. and Jackson, M.L. (1949) Mineralogical analysis of soils. *Soil Science*, **68**, 57–74.

Johansson, U., Holmgren, A., Forsling, W., and Frost, R. (1998) Isotopic exchange of kaolinite hydroxyl protons: a diffuse reflectance infrared Fourier transform spectroscopy study. *Analyst*, **123**, 641–645.

Johnston, C.T., Sposito, G., Bocian, D.F., and Birge, R.R. (1984) Vibrational spectroscopic study of the interlamellar kaolinite-dimethylsulfoxide complex. *Journal of Physical Chemistry*, **88**, 5959–5964.

Johnston, C.T., Agnew, S.F., and Bish, D.L. (1990) Polarized single-crystal Fourier-transform infrared microscopy of Ouray dickite and Keokuk kaolinite. *Clays and Clay Minerals*, **38**, 573–583.

Johnston, C.T. (2010) Probing the nanoscale architecture of clay minerals. *Clay Minerals*, **45**, 245–279.

Kittel, C. and Abrahams, E. (1953) Dipolar broadening of magnetic resonance lines in magnetically diluted crystals. *Physical Review*, **90**, 238–239.

Lagaly, G., Ogawa, M., and Dékány, I. (2013) Intercalation reactions of kaolinite. pp. 437–445 in: *Handbook of Clay Science* (F. Bergaya and G. Lagaly, editors) Developments in Clay Science, Vol. **5A**, 2nd edition. Elsevier, Amsterdam.

Langford, J.I. (1978) A rapid method for analysing the breadths of diffraction and spectral lines using the Voigt function. *Journal of Applied Crystallography*, **11**, 10–14.

Laszlo, P. (1986) Catalysis of organic reactions by inorganic solids. *Accounts of Chemical Research*, **19**, 121–127.

Ledoux, R.L. and White, J.L. (1964) Infrared study of selective deuteration of kaolinite and halloysite at room temperature. *Science*, **145**, 47–49.

Letaief, S., Diaco, T., Pell, W., Gorelsky, S.I., and Detellier, C. (2008) Ionic conductivity of nanostructured hybrid materials designed from imidazolium ionic liquids and kaolinite. *Chemistry of Materials*, **20**, 7136–7142.

Letaief, S. and Detellier, C. (2009) Clay-polymer nanocomposite material from the delamination of kaolinite in the presence of sodium polyacrylate. *Langmuir*, **25**, 10975–10979.

Letaief, S. and Detellier, C. (2011) Application of thermal analysis for the characterisation of intercalated and grafted organo-kaolinite nanohybrid materials. *Journal of Thermal and Analytical Calorimetry*, **104**, 831–839.

Li, S., Zheng, A., Su, Y., Fang, H., Shen, W., Yu, Z., Chen, L., and Deng, F. (2010) Extra-framework aluminium species in hydrated faujasite zeolite as investigated by two-dimensional solid-state NMR spectroscopy and theoretical calculations. *Physical Chemistry Chemical Physics*, **12**, 3895–3903.

Lin, F., He, L., Hou, J., Masliyah, J., and Xu, Z. (2016) Role of ethyl cellulose in bitumen extraction from oil sands ores using an aqueous-nonaqueous hybrid process. *Energy & Fuels*, **30**, 121–129.

MacKenzie, K.J.D. and Smith, M.E. (2002) Physical Background. Chapter 2, pp. 21-108, in: *Multinuclear Solid-state Nuclear Magnetic Resonance of Inorganic Materials*. (R.W. Cahn, series editor). Pergamon Materials Series, Volume 6. Elsevier Science Ltd, Oxford, UK, 748 pp.

Mansa, R., Piegang, G. B. N., and Detellier, C. (2017) Kaolinite aggregation in book-like structures from non-aqueous media. *Clays and Clay Minerals*, **65**, 193–205.

Massiot, D., Fayon, F., Capron, M., King, I., Le Calvé, S., Alonso, B., Hoatson, G., Durand, J., Bujoli, B., Gan, Z., and Hoatson, G. (2002) Modelling one- and two -dimensional solid-state NMR spectra. *Magnetic Resonance in Chemistry*, **40**, 70–76.

Mccabe R.W. and Adams, J.M. (2013) Clay minerals as catalysts. pp. 491–523, Chap 4 in: *Handbook of Clay Science* (F. Bergaya and G. Lagaly, editors). Developments in Clay Science, Vol. **5A**, 2nd ed. Elsevier, Amsterdam.

Michalková, A. and Tunega, D. (2007) Kaolinite:dimethylsulfoxide intercalate – A theoretical study. *Journal of Physical Chemistry C*, **111**, 11259–11266.

Millot, Y. and Man, P.P. (2002) Procedures for labeling the high-resolution axis of two-dimensional MQ-MAS NMR spectra of half-integer quadrupole spins. *Solid State Nuclear Magnetic Resonance*, **21**, 21–43.

Murray, H.H. and Keller, W.D. (1993) Kaolins, kaolins, and kaolins. Pp 1–24 in: *Kaolin Genesis and Utilization* (Murray, H.H., Bundy, W.M., and Harvey, C.C., editors), Special Publication No 1, The Clay Minerals Society, Boulder, Colorado, USA

Murray, H.H. (2007) *Applied Clay Mineralogy*. Developments in Clay Science, Vol 2. Elsevier, Oxford (180 pp).

Ngnie, G., Dedzo, G.K., and Detellier, C. (2016) Synthesis and catalytic application of palladium nanoparticles supported on kaolinite-based nanohybrid materials. *Dalton Transactions*, **45**, 9065–9072.

Olejnik, S., Aylmore, L.A.G., Posner, A.M., and Quirk, J.P. (1968) Infrared spectra of kaolin mineral – dimethylsulfoxide complexes. *Journal of Physical Chemistry*, **72**, 241–249.

Paris, M. (2014) The two aluminum sites in the ^{27}Al MAS NMR spectrum of kaolinite: Accurate determination of isotropic chemical shifts and quadrupolar interaction parameters. *American Mineralogist*, **99**, 393–400.

Pruett, R.J. and Webb, H.L. (1993) Sampling and analysis of KGa-1b well crystallized kaolin source clay. *Clays and Clay Minerals*, **41**, 514–519.

Raupach, M., Barron, P.F., and Thompson J.G. (1987) Nuclear magnetic resonance, infrared, and X-ray powder diffraction study of dimethylsulfoxide and dimethylselenoxide intercalates with kaolinite. *Clays and Clay Minerals*, **35**, 208–219.

Rocha, J. and Pedrosa de Jesus, D. (1994) ^{27}Al satellite transition MAS-NMR spectroscopy of kaolinite. *Clay Minerals*, **29**, 287–291.

Romo, L.A. (1956) The exchange of hydrogen by deuterium in hydroxyls of kaolinite. *Journal of Physical Chemistry*, **60**, 987–989.

Scholtzova, E. and Smrcok, L. (2009) Hydrogen bonding and vibrational spectra in kaolinite dimethylsulfoxide and dimethylselenoxide intercalates. A solid-state computational

study. *Clays and Clay Minerals*, **57**, 54–71.
Schroeder, P.A. and Erickson, G. (2014) Kaolin: from ancient porcelains to nanocomposites. *Elements*, **10**, 177–182.
Thompson, J.G. (1985) Interpretation of solid state ^{13}C and ^{29}Si nuclear magnetic resonance spectra of kaolinite intercalates. *Clays and Clay Minerals*, **33**, 173–180.
Thompson, J.G. and Cuff, C. (1985) Crystal structure of kaolinite: dimethylsulfoxide intercalate. *Clays and Clay Minerals*, **33**, 490–500.
Tonlé, I.K., Letaief, S., Ngameni, E., and Detellier, C. (2009) Nanohybrid materials from the grafting of imidazolium cations on the interlayer surfaces of kaolinite. Application as electrode modifier. *Journal of Material Chemistry*, **19**, 5996–6003.
Tonlé, I.K., Letaief, S., Ngameni, E., Walcarius, A., and Detellier, C. (2011) Square wave voltammetric determination of lead(II) ions using a carbon paste electrode modified by a thiol-functionalized kaolinite. *Electroanalysis*, **23**, 245–252.
Tunney, J.J. and Detellier, C. (1993) Interlamellar covalent grafting of organic units on kaolinite. *Chemistry of Materials*, **5**, 747–748.
Tunney, J.J. and Detellier, C. (1994) Preparation and characterization of two distinct ethylene glycol derivatives of kaolinite. *Clays and Clay Minerals*, **42**, 552–560.
Van Vleck, J.H. (1948) The dipolar broadening of magnetic resonance lines in crystals. *Physical Review*, **74**, 1168–1183.
Wang, L., Wu, D., Yuan, P., Chen, Z., and Chen, Z. (2002) ^{1}H MAS NMR spectra of kaolinite/formamide intercalation compound. *Chinese Science Bulletin*, **47**, 504–508.
Wasylishen, R.E., Ashbrook, S.E., and Wimperis, S. (2012) *NMR of Quadrupolar Nuclei in Solid Materials*. Somerset, UK: John Wiley & Sons, Inc., 550 pp.
Wojdyr, M. (2010) Fityk: a general-purpose peak fitting program. *Journal of Applied Crystallography*, **43**, 1126–1128.
Yariv, S. and Lapides, I. (2008) Thermo-infrared spectroscopy analysis of dimethylsulfoxide-kaolinite intercalation complexes. *Journal of Thermal Analysis and Calorimetry*, **94**, 433–440.
Yong, R.N. and Mourato, D. (1990) Influence of polysaccharides on kaolinite structure and properties in a kaolinite-water system. *Canadian Geotechnical Journal*, **27**, 774–788.
Zhou, B., Sherriff, B.L., and Wang, T. (2009) ^{27}Al NMR spectroscopy at multiple magnetic fields and *ab initio* quantum modeling for kaolinite. *American Mineralogist*, **94**, 865–871.
Zhu, X., Zhu, Z., Lei, X., and Yan, C. (2016) Defects in structure as the sources of the surface charges of kaolinite. *Applied Clay Science*, **124-125**, 127–136.

(*Received 27 April 2017; revised 5 July 2017; Ms. 1178; AE: G.D. Chryssikos*)